**Arecibo Observatory Technical Memo AOTM 99-02**

# THE LBW FEED: POINTING ACCURACY, BEAMWIDTH, BEAM SQUINT, BEAM SQUASH

Carl Heiles

## ABSTRACT

During February-March 1999 we made extensive observations to obtain a complete characterization of the polarization properties of the LBW feed over the frequency range $1420.4 \pm 6.25$ MHz. In a previous memo (AOTM 99-01) we presented our scheme of Mueller matrices. Here we present the polarized beam patterns and, as a by product, pointing accuracy.

The executive summary of this report is a succinct six sentences:

**(1)** The system temperature in each polarization channel increases with zenith angle and ranges from about 36 to 40 Kelvins.

**(2)** The pointing errors have a systematic offset in zenith angle and a random component. The total standard deviation, including both components, is $< 8.9''$. This is astronomically negligible.

**(3)** The beam shape is elliptical, with ellipticity changing quadratically with $za$; the ellipse is aligned with $(az, za)$. For $za = 11°$, HPBW$_{za}$ is minimum at $3.66'$ and HPBW$_{az}$ maximum at $3.14'$. At $za = 20°$ these numbers become $3.92'$ and $2.87'$, respectively.

**(4)** The beam squint in Stokes $V$ is about $1.3''$ for $za \lesssim 16°$ and rises steeply to $3.2''$ at $za = 20°$. Its direction also changes with $za$, with a total range $\sim 60°$. Beam squint is a problem in Zeeman splitting measurements; this is more than acceptably small. The beam squash in Stokes $V$ is negligible, but the Stokes $V$ HPBW is systematically larger than the Stokes $I$ HPBW by $0.61'' \pm 0.13''$.

**(5)** The beam squint in Stokes $Q$ and $U$ is about $1.8''$. The directions differ by about $100°$, and they both rotate with $za$ over a total range of about $60°$. Beam squint in linear polarization is unexpected.

**(6)** The beam squash in Stokes $Q$ and $U$ is about $3''$, independent of $za$; the position angles differ by $45°$, as expected. There is also a systematic difference in HPBW, independent of position angle, with the HPBW in Stokes $U$ larger by about $1.6''$.

## 1. GENERAL METHODOLOGY

This memo observationally derives the properties of the LBW beam. The observations consist of scans oriented at four position angles across continuum sources. We assume an elliptical Gaussian beam at arbitrary position angle, so the Stokes $I$ scans should follow a Gaussian whose offset and beamwidth reflect the pointing error and beam shape. In the other Stokes parameters the beam is described by beam squint and squash, which we define below. Section 2 develops the expected behavior of the measured Stokes parameters along a scan and section 3 the measurement technique. Section 4 presents the results.

## 2. BEAM PARAMETERS

### 2.1. Definition of beam parameters and coordinate system

The beam properties include pointing error, beamwidth, squint, and squash. Pointing error and beamwidth are familiar concepts and we won't define them; we define the others below. All the beam properties have a magnitude and direction, and we will assume that they are fixed with respect to azimuth and zenith angle.

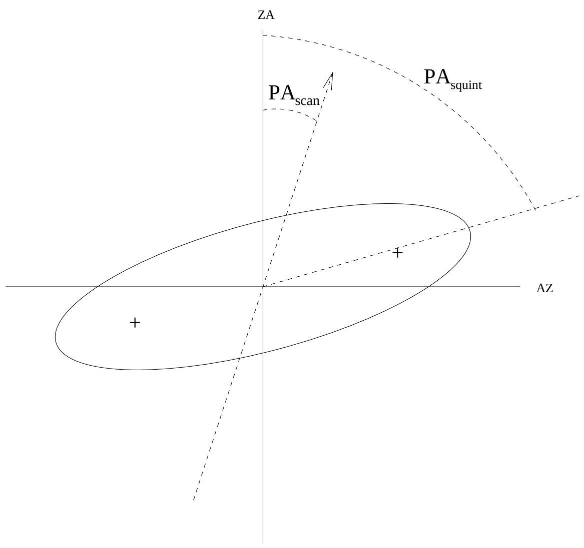


Fig. 1.— Schematic illustration of beam squint. The $ZA$ axis is the zenith angle direction and corresponds physically to the azimuth arm. $PA_{squint}$ refers to the position angle of the squint and $PA_{scan}$ to that of a line along which observations are taken. Clearly, observed effects change as $\cos(PA_{scan} - PA_{squint})$. A similar diagram and equation apply for pointing error.

We will discuss observations taken along a line oriented at an angle $PA_{scan}$ with respect to to the azimuth arm, measured towards increasing azimuth (towards the East). This is illustrated explicitly in Figure 1. Azimuth increases towards the east, which is the same sense as $PA_{scan}$, so for the position angle on the sky these two angles add. Roughly the azimuth arm has $PA_{az} \approx az - 180°$. Thus the position angle of our scan on the sky is $PA_{sky} = PA_{az} + PA_{scan} \approx (az + PA_{scan} - 180°)$. In our calculations we use the exact equation, not the approximation.

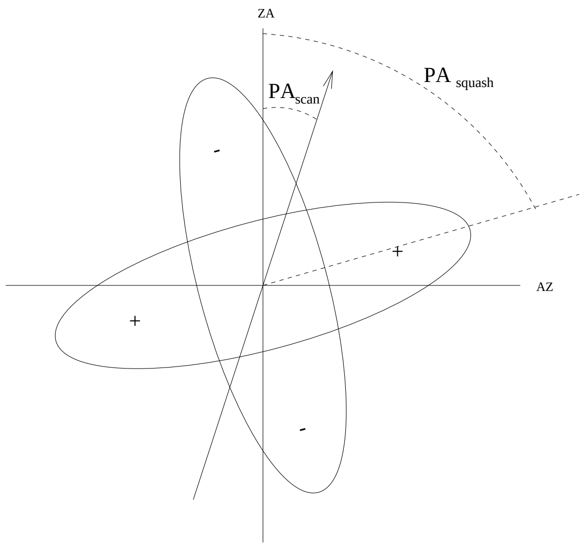


Fig. 2.— Schematic illustration of beam squash. The $ZA$ axis is the zenith angle direction and corresponds physically to the azimuth arm. $PA_{squash}$ refers to the position angle of the squash and $PA_{scan}$ to that of a line along which observations are taken. Clearly, observed effects change as $\cos 2(PA_{scan} - PA_{squash})$. A similar diagram and equation apply for telescope beamwidth.

One can usually obtain nearly perfect polarization performance for a point source at beam center by deriving and applying the Mueller matrix. A previous memo (AOTM 99-01) derived this matrix for the LBW feed. However, away from beam center various symmetries of the telescope are broken, and this produces polarization within the main beam. There are two kinds of beam polarization that are predicted theoretically:

**(1)** *Beam squint* occurs when the two circular polarizations point in different directions by angle $\Psi$. This makes the beam of the Stokes $V$ parameter look like the first derivative of the Stokes $I$ beam. It produces a "two-lobed" pattern, one positive and one negative, as we show schematically in Figure 1. One measures beam squint by observing Stokes $V$ along a line, the scan direction; beam squint produces a $-/+$ pattern with amplitude $\propto \cos(PA_{scan} - PA_{squint})$.

**(2)** *Beam squash* occurs when the two linear polarizations have different beamwidths by amount $\Upsilon$. This makes the beams of the Stokes $Q$ and $U$ parameters look roughly like the second derivative of the Stokes $I$ beam. These are "four-lobed" beams, in which two lobes on opposite sides of the beam center have the same sign and two lobes rotated 90° have the opposite sign, as we show schematically in Figure 2. One measures beam squash by observing Stokes $Q$ or $U$ along a line, the scan direction; beam squash produces a +/0/+ pattern with amplitude $\propto \cos 2(PA_{scan} - PA_{squash})$.

Practice does not always follow theory, and this is true for Arecibo's beam: there is significant beam squint in the linear polarizations.

We know of no theories that explicitly address polarization outside of the main beam. However, as we move further away from beam center the symmetries are broken more strongly. Thus we expect the diffraction sidelobes to be increasingly polarized with distance from beam center. In addition, there are additional sidelobes that are inherently unpredictable because they result mainly from telescope surface roughness and scattering off of the telescope support structures.

### 2.2. The definitions of Stokes Q, U, V

In this memo we use the astronomically-defined Stokes parameters $\mathbf{S_{astr}}$, whose derivation is discussed in AOTM (99-01). These Stokes parameters are defined so that position angle 0° is aligned with the azimuth arm. That is, they are consistent with the definition of $PA_{scan}$ in Figures 1 and 2. This means that Stokes $Q$, as used herein, is the product of the two linear probes and $U$ is the difference; this is in contrast to the definition used by the datataking software. Stokes $V$ is defined in the usual way, as $LCP - RCP$ from the sky.

In the terms of AOTM (99-01), this means that we have applied the total matrix correction in equation (13) of that memo. We have verified these definitions astronomically.

### 2.3. Mathematical description of the Stokes I beam parameters

Let $R_I$ be the directional response of the beam to Stokes parameter $I$; for the other Stokes parameters we use appropriate subscripts. The parameters of $R_I$ include a pointing error, which has two-lobed symmetry and is squintlike, and an elliptical beam, which has four-lobed symmetry and is squashlike. The beam is Gaussian, so for observations along a line at position angle $PA_{scan}$ we expect the observed Stokes $I$ to be

$$R_I = I_{src}\mathcal{G} = I_{src} \exp - \left[ \frac{(\theta_{scan} - \delta\Theta(PA))^2}{\Delta\Theta(PA)^2} \right] , \tag{1}$$

where $I_{src}$ is the Stokes $I$ of the source and $\theta_{scan}$ is the angle along the scan line measured from the nominal beam center and increasing towards the direction of $PA_{scan}$. Later we use the symbol

$\mathcal{G}$ as shorthand for the Gaussian. $\Delta\Theta(PA)$ depends on $PA$ because the beam is elliptical. We expect the pointing offset and beamwidth to vary as

$$\delta\Theta(PA) = \Psi_{pointing} \cos(PA_{scan} - PA_{pointing}) \tag{2a}$$

$$\Delta\Theta(PA) = \Delta\Theta_0 + \Upsilon_{beam} \cos 2(PA_{scan} - PA_{beam}) \; . \tag{2b}$$

Here $\Psi_{pointing}$ is the total pointing offset and $PA_{pointing}$ its position angle. The HPBW is numerically related to $\Delta\Theta$ by the usual factor $2(\ln 2)^{1/2}$, so we have for example

$$HPBW_{az\ direction} = 1.665(\Delta\Theta_0 - \Upsilon_{beam} \cos 2PA_{beam}) \tag{3a}$$

$$HPBW_{za\ direction} = 1.665(\Delta\Theta_0 + \Upsilon_{beam} \cos 2PA_{beam}) \tag{3b}$$

Note this important point: $R_I$ varies as $\cos(2PA)$ instead of $\cos(PA)$. This means that if the beam is not aligned with the $(az, za)$ directions, then observations taken in these directions alone will not reveal the misalignment. As it happens, the alignment is good, but perhaps not perfect.

We take data along a line, called a scan, at position angle $PA_{scan}$. For each scan, we least-square fit equation 1 plus a constant to obtain $\delta\Theta(PA)$ and $\Delta\Theta(PA)$. We have many scans at four different $PA$'s. We then least square fit all these data with equation 2 to obtain $(\Psi_{pointing}, PA_{pointing})$ and, also, the HPBW and its $PA$.

### 2.4. Mathematical description of the Stokes Q, U, V beam parameters

Let $D_P$ be the directional response of the beam to a particular polarization $P$; here $P$ can be one of the circular polarizations or a linear polarization. These combine in pairs to form Stokes parameter beams, which we designate by the letter $R$.

Here we write equations only for circular polarization, but similar equations apply to the other polarizations. For observations along a line at position angle $PA_{scan}$ the beam squint and squash distort the beam as follows:

$$D_{LCP} = LCP_{src} \exp - \left[ \frac{(\theta'_{scan} + \frac{\psi(PA)}{2})^2}{(\Delta\Theta(PA) + \frac{\Upsilon(PA)}{2})^2} \right] \tag{4a}$$

$$D_{RCP} = RCP_{src} \exp - \left[ \frac{(\theta'_{scan} - \frac{\psi(PA)}{2})^2}{(\Delta\Theta(PA) - \frac{\Upsilon(PA)}{2})^2} \right] \tag{4b}$$

Here, for each scan $\theta'_{scan} = \theta_{scan} - \delta\Theta(PA)$, with $\delta\Theta(PA)$ and $\Delta\Theta(PA)$ determined following section 2.3. The Stokes $I$ beam $R_I$ is the sum, in which the beam squint and squash drop out to first order. The Stokes $V$ beam is the difference; because the beam squint and squash are small quantities linear expansions are adequate, so we have

$$R_V(\theta_{scan}) = \frac{V_{src}}{I_{src}} R_I + \frac{1}{2} \left( \frac{\partial R_I}{\partial \psi(PA)} \psi(PA) + \frac{\partial R_I}{\partial \Upsilon(PA)} \Upsilon(PA) \right) , \tag{5}$$

where $\frac{V_{src}}{I_{src}}$ is the fractional circular polarization. As with the Stokes $I$ parameter, we expect

$$\Psi(PA) = \Psi_V \cos(PA_{scan} - PA_{\Psi_V}) \tag{6a}$$

$$\Upsilon(PA) = \Upsilon_V \cos 2(PA_{scan} - PA_{\Upsilon_V}) \; . \tag{6b}$$

We treat the polarized Stokes parameter data as we did the Stokes $I$ data. For each scan, we first obtain the beam parameters and $I_{src}$ from the Stokes $I$ fit. We use those parameters in equation 5 plus a constant and least-squares fit for $\psi(PA)$ and $\Upsilon(PA)$. We have many scans at four different $PA$'s. We then least square fit these data with equation 6 to obtain $\Psi_V$, $\Upsilon_V$, and their associated position angles.

## 3. MEASUREMENT TECHNIQUE

### 3.1. The "chcross" observing procedure and its data reduction

We observed a good sample of sources using the "chcross" observing procedure, which samples 7 points in each of two orthogonal directions on the sky. The central point is the peak of the source. Its nearest neighbors are the offsets where the first derivatives of the Gaussian $\left|\frac{\partial \mathcal{G}}{\partial \Theta}\right|$ are maximum. The next neighbors are where derivatives $\left|\frac{\partial \mathcal{G}}{\partial (\Delta\Theta)}\right|$ are maximum. The outermost points are far enough away to act as suitable off positions. In observing we assumed HPBW of $3.5'$ for all $PA_{scan}$ and used offsets of $\pm(.425, .736, 1.27)$HPBW.

Our crosses were oriented both aligned with $(az, za)$ and also at $45°$, i.e. at $PA_{scan} = 0°, 45°, 90°, 135°$. We repetitively measured these crosses over the full tracking range of each source. We used the correlator in Stokes mode. Before processing any data we first corrected with the Mueller matrix described in our previous memo.

For each 7-point set we first fit the Gaussian in equation 1, plus a constant, to the Stokes $I$. The constant is the off-source system temperature and the Gaussian parameters are the source deflection, position error, and beamwidth. Denote this Gaussian by $R_I$, as in equation 1; note that it is an observed quantity with 7 points, and because it is derived from the fit to Stokes $I$ it is derived with high precision but its intensity scale is inaccurate because of the zenith angle gain variation. We then fit the 7 points in the other Stokes parameters with equation 5 plus a constant. The coefficient of the constant term is an offset with units of Kelvins; it is the polarized emission produced by the losses or reflections in the feed.

### 3.2. Astronomical source selection

We observed 15 sources with the chcross procedure: 3C33, 3C41, 3C98, 3C138, P0736+01, 3C223, 3C234, 3C274.1, 3C286, P1414+11, 3C336, 3C386, 3C399.1, CTA102, 3C454.3. 3C336 was inadvertently omitted from all of our data reduction. We wanted to include as many sources as possible to increase the $(az, za)$ coverage. However, some are partially resolved in some Stokes parameters which made them unsuitable for deriving some beam parameters; we comment on this in each section below.

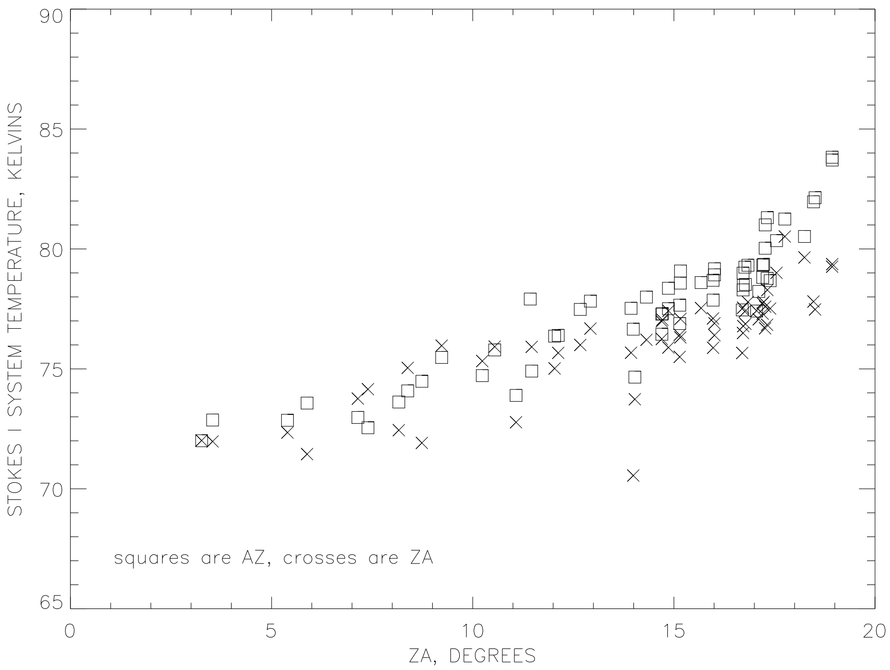


Fig. 3.— Stokes $I$ system temperature versus $za$.

## 4. THE BEAM PROPERTIES IN STOKES I

### 4.1. Off-source system temperature in Stokes I

Figure 3 exhibits the off-source Stokes $I$ system temperature versus zenith angle; squares refer to the $az$ direction ($PA_{scan} = 90°$) and crosses to $za$ ($PA_{scan} = 0°$). This figure includes only those sources with flux density $< 10$ Jy to avoid a small nonlinear calibration problem. The crosses exhibit systematically smaller system temperatures. This behavior is mystifying because the crosses are derived from $za$ scans. The $za$ HPBW is larger than the $az$ HPBW, so one would expect the $az$ off-source points to have a smaller residual source contribution and thus a smaller system temperature, contrary to the observations.

One should estimate a lower envelope in Figure 3 to avoid contributions from the sources themselves. The Stokes $I$ system temperature decreases monotonically with $za$, reaching a minimum of about 72 Kelvins and rising to about 80 Kelvins at $za = 20°$. These are twice the system temperature in each polarization channel.

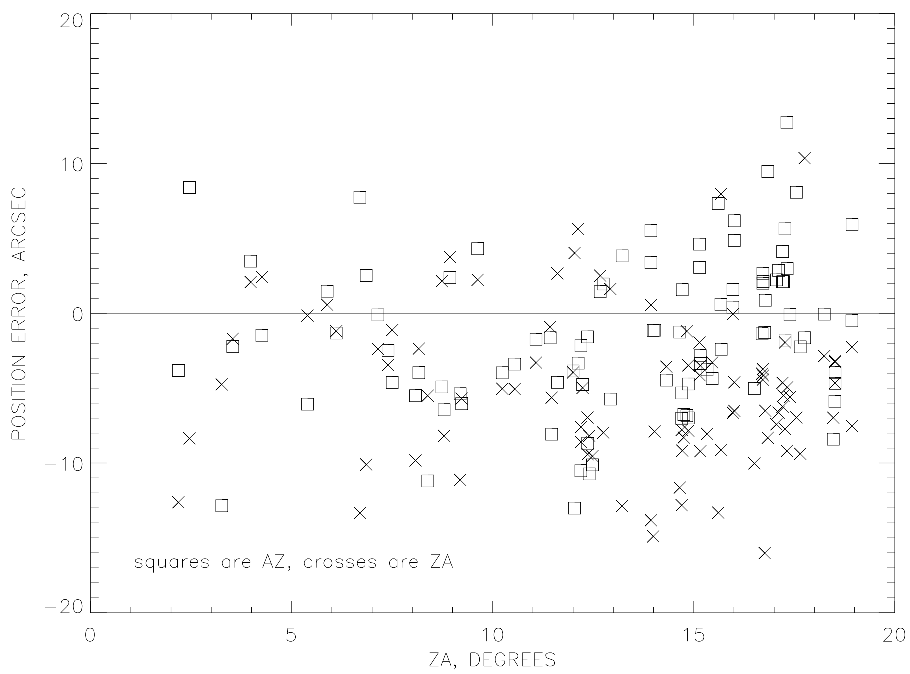


Fig. 4.— Pointing errors in the $az$ (squares) and $za$ (crosses) directions versus $za$.

### 4.2. Pointing accuracy

We included all sources except 3C33, even the partially resolved ones, because their centroid positions are well defined. Figure 4 exhibits the pointing errors versus zenith angle; squares refer to the $az$ direction and crosses to $za$. The squares might show some $za$ dependence at the level of a few arcsec. For all squares the mean is $-1.4 \pm 0.6''$ and the standard deviation is $5.1''$. The crosses are systematically negative, particularly at low $za$. The mean of all crosses is not representative because it is highly weighted by the higher $za$'s, where the position error becomes less negative; this mean is $-5.1'' \pm 0.5''$ and the standard deviation is $5.0''$. We emphasize that these standard deviations do not include the contributions from **(1)** the catalog positions, which are from BDFL (1972), and **(2)** the observations themselves; they are therefore upper limits.

Adding all pointing errors quadratically, including the systematic offsets, yields a standard deviation of $< 8.9''$; excluding the systematic offsets yields $< 7.1''$. Again, we emphasize that these are upper limits. Our main purpose is not to determine accurate pointing information so we are not inclined to delve into these details. The important statement is the astronomical one: these pointing errors are negligible!

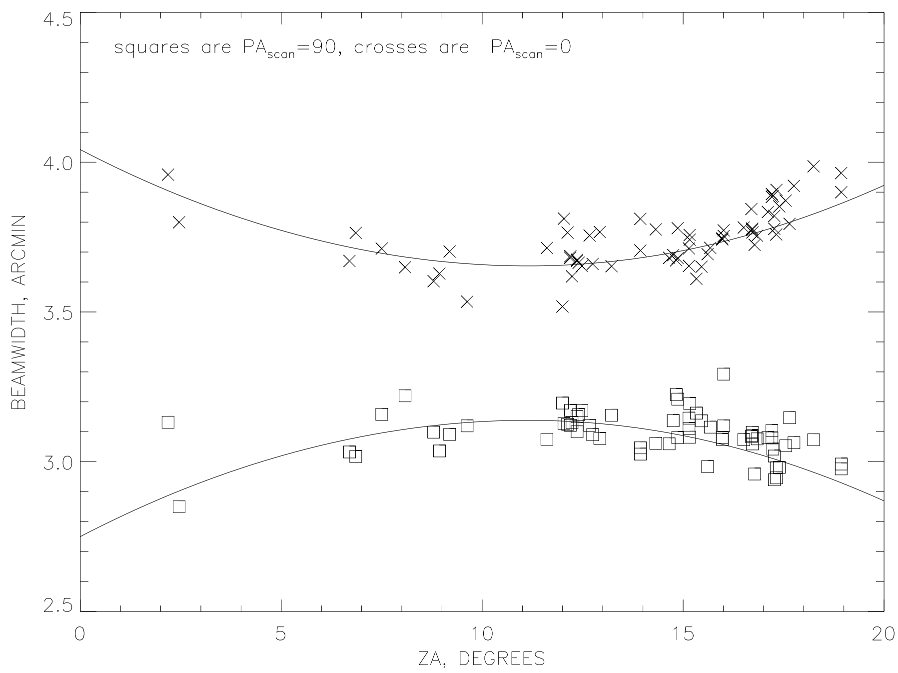


Fig. 5.— HPBWs in the $az$ (squares) and $za$ (crosses) directions versus $za$; solid lines are the fits of equation 7.

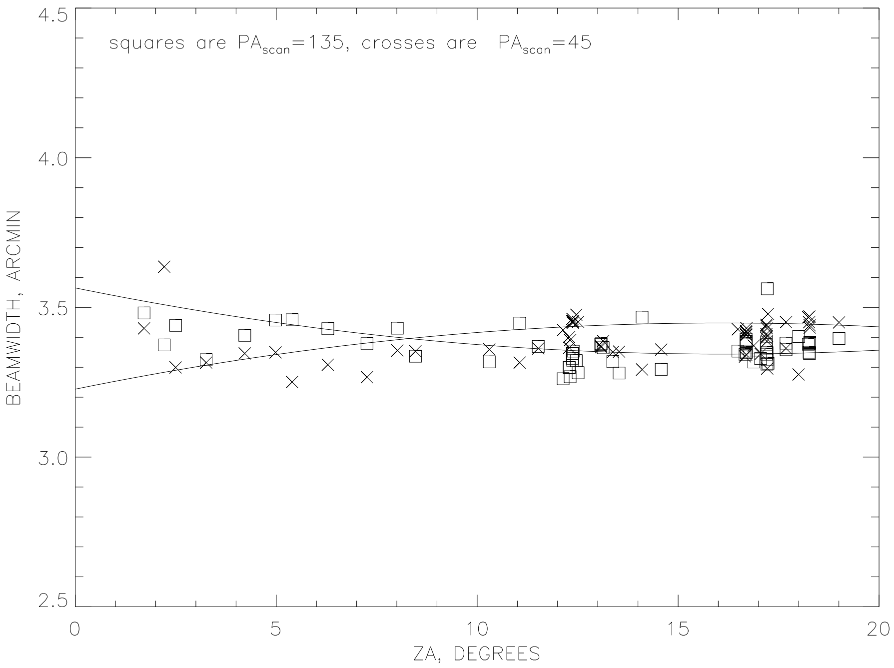


Fig. 6.— HPBWs at 45° to the $(az, za)$ directions; solid lines are the fits of equation 7. These HPBWs are almost equal, showing that the elliptical beam is well-aligned with these directions.

### 4.3. HPBW

We excluded partially resolved sources, leaving us with the following: 3C41, 3C138, P0736+01, 3C286, 3C336, 3C399.1, CTA102, 3C454.3. Figure 5 exhibits the HPBW versus zenith angle in the cardinal $(az, za)$ directions. Squares refer to the $az$ direction ($PA_{scan} = 90°$) and crosses to $za$ ($PA_{scan} = 0°$). Both have a quadratic-like $za$ dependence, with the $az$ beamwidth decreasing and the $za$ beamwidth increasing at low and high $za$. Figure 6 exhibits the HPBW versus zenith angle at 45° to the cardinal $(az, za)$ directions; the near-equality of these HPBWs shows that the beam is well-aligned with the cardinal directions. Moreover, the opposite $za$ dependences of the HPBWs in Figure 5 conspire to make these HPBWs more nearly independent of $za$.

We least-square fit the data to equation 2b, with each coefficient being a second-degree polynomial in in $za_{10} = (za - 10°)$. We found that $|PA_{beam}| < 7°$; although the departure from zero is formally larger than the errors, the incomplete coverage in $(az, za)$ makes this departure questionable so we take $PA_{beam} = 0°$ for simplicity. With this, the HPBW is well represented by the solid lines in Figures 5 and 6 and the following equations:

$$HPBW = (3.396 \pm 0.004) + H(za)\cos(2PA_{scan}) \tag{7a}$$

$$H(za) = (0.262 \pm 0.009) - \frac{0.067 \pm 0.019}{10} za_{10} + \frac{0.33 \pm 0.03}{100} za_{10}^2 \,. \tag{7b}$$

The narrowest HPBW$_{za}$ occurs at $za = 11°$, where the HPBWs are $(3.136', 3.655')$ for $(az, za)$.

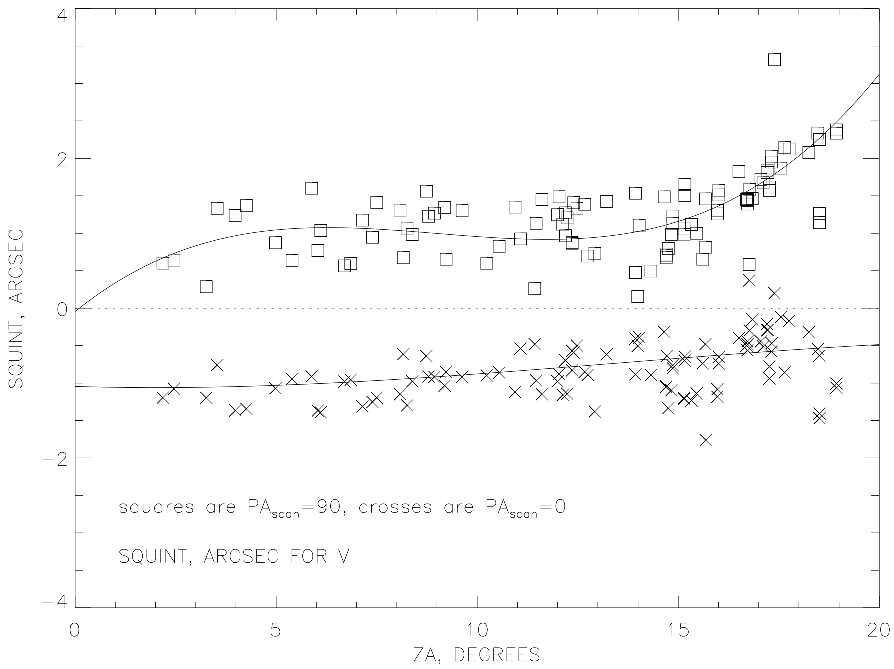


Fig. 7.— Stokes $V$ beam squint in the $az$ (squares) and $za$ (crosses) directions versus $za$; solid lines are the fits of equation 8.

## 5. THE BEAM PROPERTIES IN STOKES V

Astronomical sources exhibit very little circular polarization and all sources were useful for deriving the Stokes $V$ squint and squash.

### 5.1. Squint

Figure 7 exhibits the Stokes $V$ squint versus zenith angle; squares are for the $az$ direction with $PA_{scan} = 90°$ and crosses the $za$ direction with $PA_{scan} = 0°$. The $za$ squint is roughly independent of $za$. The $az$ squint is roughly constant for $za \lesssim 16°$; then it increases sharply. This behavior is expected theoretically. First, recall the situation for a prime-focus feed: if the feed points away from the center of symmetry in a particular direction, beam squint is produced in the orthogonal direction. At Arecibo, for high $za$ the dish illumination pattern becomes asymmetric in the $za$ direction, so this should cause a squint in the $az$ direction.

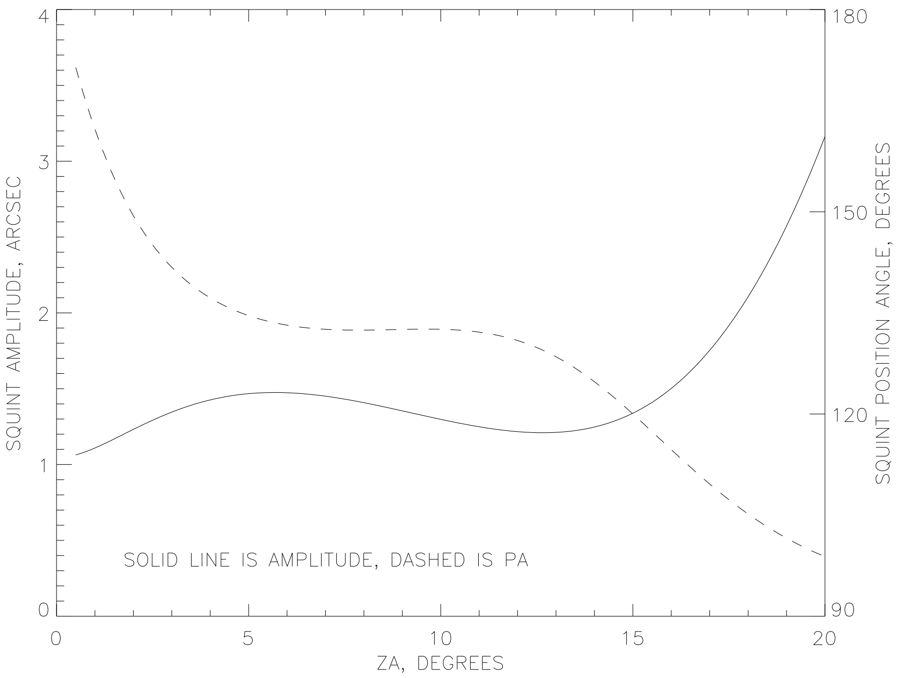


Fig. 8.— Stokes $V$ beam squint from equation 8 with parameters in the form of equation 6a.

We also obtained chcross data at 45° to the $(az, za)$ directions. We least-square fit all data to equation 6a (actually, to its $\cos + \sin$ counterpart), with each coefficient being a third-degree polynomial in $za_{10} = (za - 10°)$. The Stokes $V$ squint is shown by the solid lines in Figure 8 and given by (units are arcseconds)

$$\Psi_V = \Psi_{cos}(za)\cos(PA_{scan}) + \Psi_{sin}(za)\sin(PA_{scan}) \tag{8a}$$

$$\Psi_{cos} = (-0.88 \pm 0.04) + \frac{0.39 \pm 0.13}{10} za_{10} + \frac{0.11 \pm 0.15}{100} za_{10}^2 + \frac{-0.11 \pm 0.27}{1000} za_{10}^3 \tag{8b}$$

$$\Psi_{sin} = (0.96 \pm 0.04) + \frac{-0.38 \pm 0.13}{10} za_{10} + \frac{0.58 \pm 0.15}{100} za_{10}^2 + \frac{1.96 \pm 0.27}{1000} za_{10}^3 \quad (8c)$$

Figure 8 exhibits this dependence, as parameterized in the form of equation 6a. The beam squint is typically $\sim 1.4''$, smaller than for any other telescope ever used for measuring Zeeman splitting of the 21-cm line (Heiles 1996); after correction, its effects will be unimportant.

### 5.2. Squash

There is no statistically significant beam squash for Stokes $V$. However, we were surprised to find the Stokes $V$ HPBW to be systematically larger than the Stokes $I$ HPBW by $0.61'' \pm 0.13''$, independent of $PA_{scan}$.

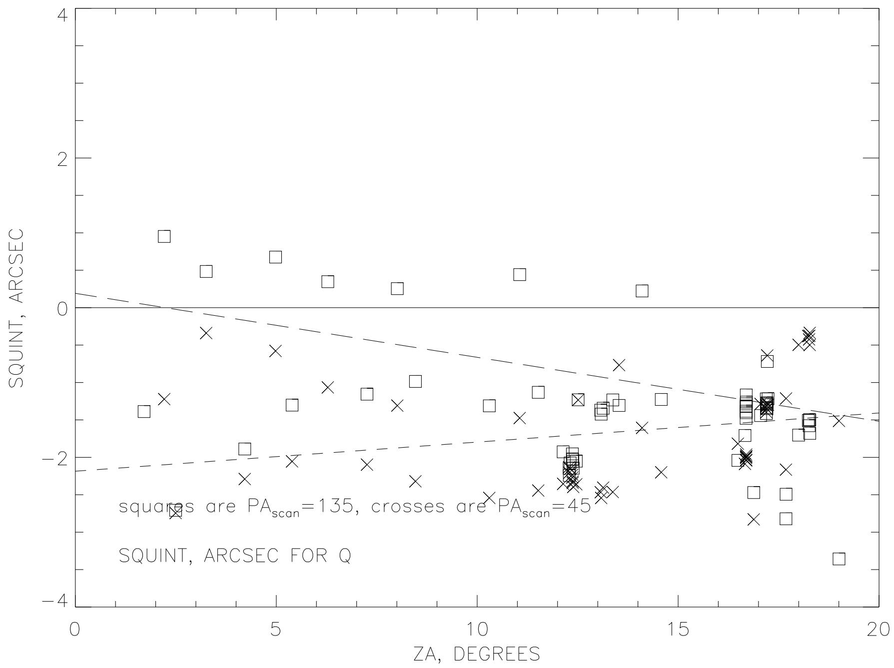


Fig. 9.— Stokes $Q$ beam squint at 45° to the cardinal $(az, za)$ directions versus $za$. Dashed lines are the fits of equation 9. The see-saw behavior of points for $az < 12°$ is an intrinsic effect of 3C138 (see text).

## 6. THE BEAM PROPERTIES IN STOKES Q AND U

Beam measurements for Stokes $Q$ and $U$ are greatly complicated by the fact that astronomical sources have not only significant linear polarization, but also angular structure in linear polarization. We found many sources to have significant intrinsic squint and squash. We went to a great deal of trouble to examine each source individually to determine its suitability as a calibrator.

Stokes $Q$ is derived from the difference between the two linear polarizations. The usual opinion is that it is therefore inaccurate and noisy. However, we found it to be accurate and only somewhat noisier than Stokes $U$. This bespeaks the accuracy of our Mueller matrix correction and, in addition, the stability of the calibration noise diodes.

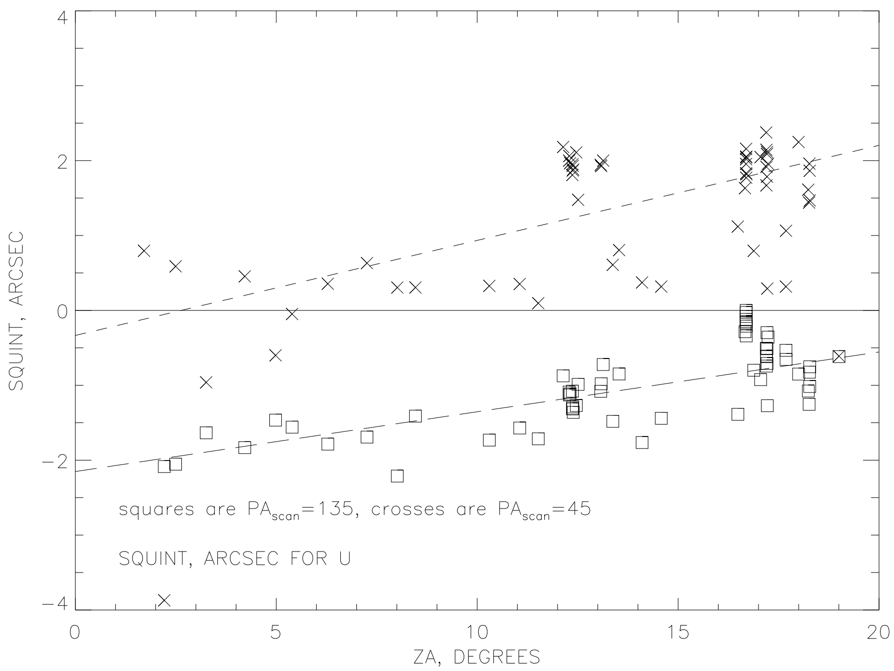


Fig. 10.— Stokes $U$ beam squint at 45° to the cardinal $(az, za)$ directions versus $za$. Dashed lines are the fits of equation 10.

### 6.1. Squint

We excluded sources that exhibited deleterious intrinsic squint. Some exhibited benign intrinsic squint, meaning that it was recognizable but the data were consistent with the other data. We used sources 3C41, 3C138, P0736+01, 3C286, 3C399.1, CTA102, 3C454.3.

Figure 9 exhibits the Stokes $Q$ and $U$ squint versus zenith angle for scans in the cardinal directions; Figure 10 is for the 45° directions. We least-square fit the data to equation 6b (actually, to its cos + sin counterpart), with each coefficient being a first-degree polynomial in $za_{10} = (za - 10°)$. The fits are shown by the dashed lines in Figures 9 and 10. For Stokes $Q$ we have (units are arcseconds)

$$\Psi_Q = \Psi_{Qcos}(za)\cos(PA_{scan}) + \Psi_{Qsin}(za)\sin(PA_{scan}) \tag{9a}$$

$$\Psi_{Qcos} = (-0.80 \pm 0.09) + \frac{0.87 \pm 0.16}{10} za_{10} \tag{9b}$$

$$\Psi_{Qsin} = (-1.73 \pm 0.09) + \frac{-0.33 \pm 0.16}{10} za_{10} \tag{9c}$$

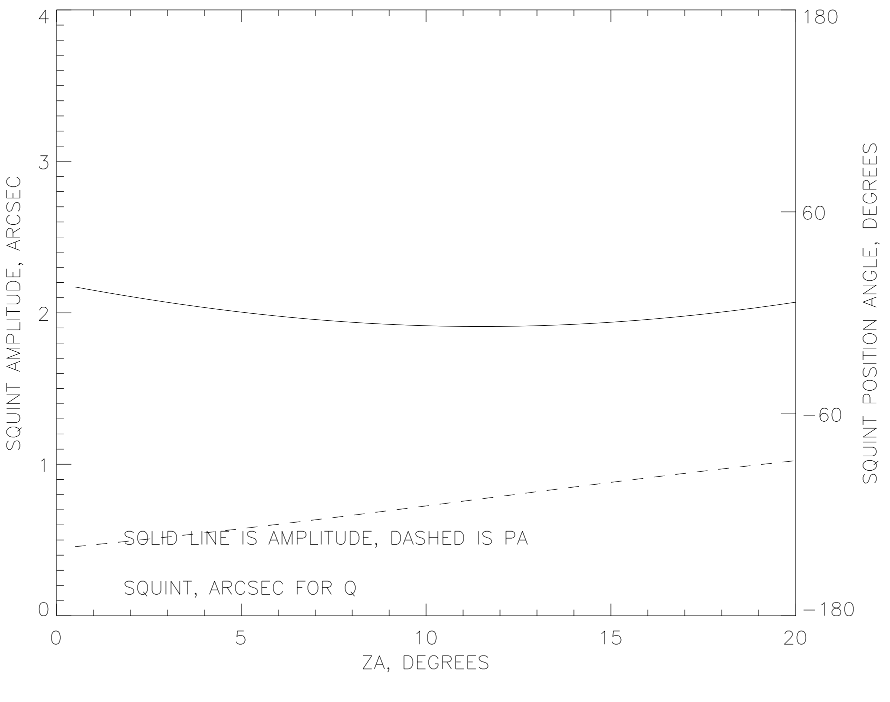


Fig. 11.— Stokes $Q$ beam squint from equation 9 with parameters in the form of equation 6a.

and for Stokes $U$

$$\Psi_U = \Psi_{Ucos}(za)\cos(PA_{scan}) + \Psi_{Usin}(za)\sin(PA_{scan}) \tag{10a}$$

$$\Psi_{Ucos} = (1.62 \pm 0.08) + \frac{0.33 \pm 0.14}{10} za_{10} \tag{10b}$$

$$\Psi_{Usin} = (-0.30 \pm 0.08) + \frac{1.46 \pm 0.14}{10} za_{10} \tag{10c}$$

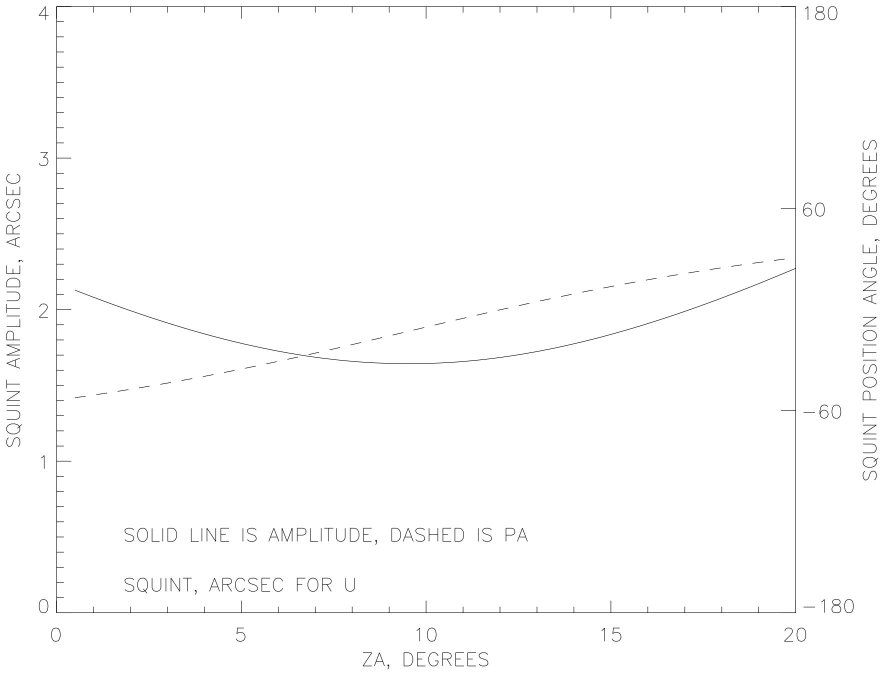


Fig. 12.— Stokes $U$ beam squint from equation 10 with parameters in the form of equation 6a.

Figures 11 and 12 exhibit this dependence, as parameterized in the form of equation 6a.

Theoretically, one doesn't expect beam squint in linear polarization. One might argue that it somehow arises from passage through the telescope support structure; however, if this were the case one would expect it to depend on telescope azimuth and/or zenith angle. We found no discernible dependence on either coordinate (but we must comment that our $(az, za)$ coverage is insufficiently complete to rule out such dependence). Similarly, one expects an effect like this from the angular polarization structure of continuum sources. In fact, these effects are clear for some of our sources; they vary as $\cos(PA_{sky})$ instead of $\cos(2PA_{sky})$, which means that the parallactic angle doesn't change enough to get a reliable fit. An example is in figure 9: the see-saw behavior of points for $az < 12°$ are 3C138 on opposite sides of transit, which have $PA_{sky}$ different by $\sim 160°$. These intrinsic source effects contribute to the scatter in the figures, but the instrumental effect dominates. Thus, the linear polarization beam squint is tied mainly to the receiver, not to the sky or the telescope support structure.

It is conceivable that this effect arises from a difference in physical location of the phase centers of the two linear probes in the feed. With Arecibo's focal length $\sim$ 500 m, a $1''$ angle corresponds to a linear distance of only 1.2 mm in the focal plane. It is clear that this would produce a beam squint in Stokes $U$, which is the difference between the two probes. But it isn't clear (to us, at any rate) what such a difference should produce in Stokes parameters $Q$ and $V$, or for beam squash. We note that the difference $PA_{\Psi_Q} - PA_{\Psi_U}$ varies from $86° \rightarrow 118°$, which is fairly close to 90°.

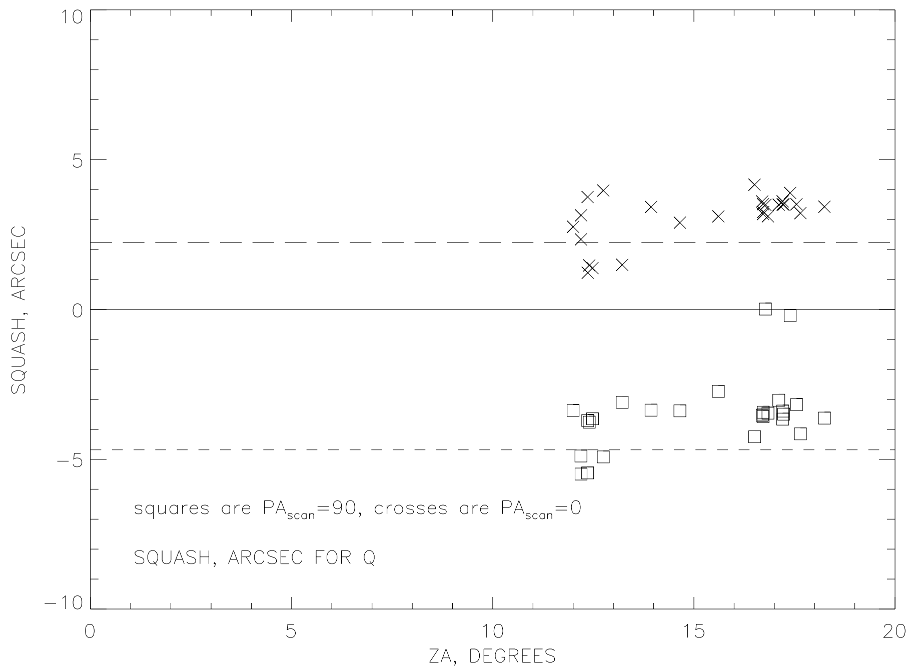


Fig. 13.— Stokes $Q$ beam squash in the $az$ (squares) and $za$ (crosses) directions versus $za$.

## 6.2. Squash

All but three sources exhibited unacceptably large intrinsic squash in linear polarization. 3C386 was particularly extreme with an intrinsic squash $\sim 5''$. The preponderance of intrinsic squash is undoubtedly a reflection of the structure of typical radio galaxies: two highly linearly polarized lobes are the very definition of squash. The only sources we included here are 3C138, P0736+01, 3C286.

Figures 13 and 14 exhibit the squash in Stokes $Q$ and $U$. Figure 14 is for the chcross procedure at 45° with respect to $(az, za)$, while Figure 13 is for chcross aligned. We pick these to illustrate the four-lobed symmetry of the squash: the four lobes rotate 45° between these two Stokes parameters. The difference in squash between squares and crosses peaks for the directions shown and goes to zero for the other directions. However, the squash itself doesn't go to zero for the other directions, which means that there is a constant offset in the squash that is independent of $PA_{scan}$.

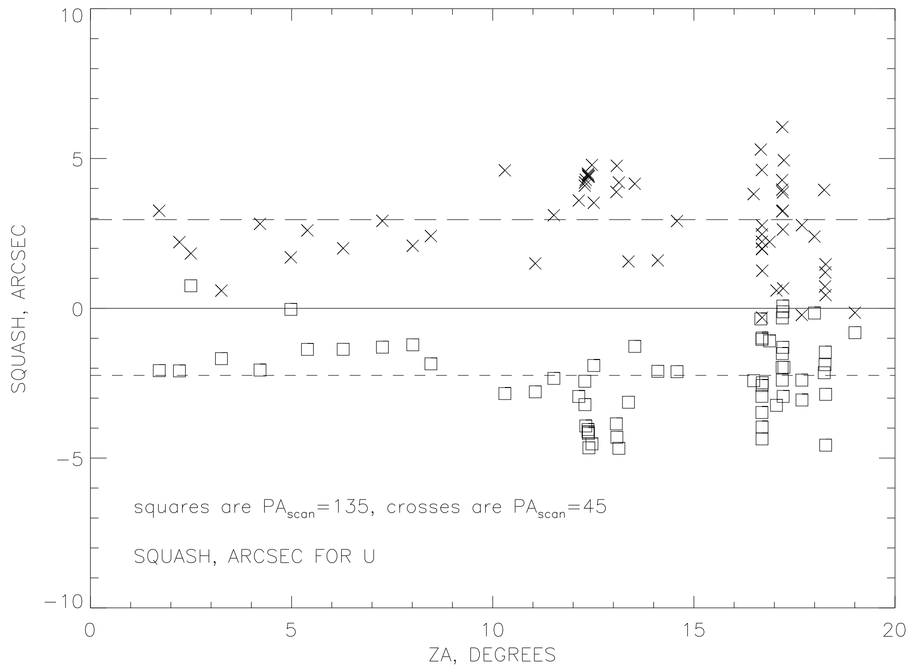


Fig. 14.— Stokes $U$ beam squash in the $az + 45°$ (squares) and $za + 45°$ (crosses) directions versus $za$.

We least-squares fit data at all $PA_{scan}$ to equation 2b (actually, to its cos + sin counterpart), with each coefficient being a constant, independent of $za$. The fits are shown by the dashed lines in Figures 13 and 14. For Stokes $Q$ we have (units are arcseconds)

$$\Upsilon_Q = (-1.23 \pm 0.07) + (3.46 \pm 0.13)\cos 2[PA_{scan} - (0.3° \pm 0.7°)] \tag{11a}$$

$$\Upsilon_U = (0.36 \pm 0.11) + (2.59 \pm 0.13)\cos 2[PA_{scan} - (44.9° \pm 2.1°)] \tag{11b}$$

The directions are as expected. Consider linear polarization near the wall of circular waveguide or a circular horn. On a radius perpendicular to E-field, the E-field is shorted out by the wall, but 90° away it is not. Looking end-on at the circular waveguide the E-field amplitude is roughly elliptical, with the narrower size in the direction perpendicular to E. This translates into a broader illumination of the dish surface and a narrower HPBW. Thus the wider HPBW lies in the direction parallel to the E-field, meaning that the Stokes $Q$ HPBW should be wider towards $PA_{scan} = 0°$. That is, the Stokes $Q$ squash should be oriented towards $PA_{scan} = 0°$ and the $U$ squash towards $PA_{scan} = 45°$, as observed.

One would expect coefficients of the $\cos(2PA_{scan})$ term to be equal for the Stokes $Q$ and $U$; they are not. Moreover, one would not expect the constant terms to be statistically significant; they are. The constant terms mean that the Stokes $U$ beam is systematically larger than the Stokes $U$ beam at all position angles. We found a similar effect for Stokes $V$. As we remarked earlier, observation does not always correspond to theory.

It is a pleasure to thank Phil Perillat for providing the excellent observing software and critical, stimulating comments; and Mike Davis for general assistance and advice.

## REFERENCES

Bridle, A.H., Davis, M.M., Fomalont, E.B., and Lequeux, J. 1972, AJ, 77, 405.

Heiles, C. 1996, ApJ, 466, 224.

Heiles, C. and Fisher, R. 1999, Green Bank Tech Memo, in preparation.